© 2017. Published by The Company of Biologists Ltd | Development (2017) 144, 4328-4335 doi:10.1242/dev.154823

RESEARCH REPORT

Microfluidic chest cavities reveal that transmural pressure controls the rate of lung development

Celeste M. Nelson[1,2,§], Jason P. Gleghorn[1,*,‡], Mei-Fong Pang[1,‡], Jacob M. Jaslove[2], Katharine Goodwin[3], Victor D. Varner[1], Erin Miller[4], Derek C. Radisky[4] and Howard A. Stone[5]

ABSTRACT

Mechanical forces are increasingly recognized to regulate morphogenesis, but how this is accomplished in the context of the multiple tissue types present within a developing organ remains unclear. Here, we use bioengineered 'microfluidic chest cavities' to precisely control the mechanical environment of the fetal lung. We show that transmural pressure controls airway branching morphogenesis, the frequency of airway smooth muscle contraction, and the rate of developmental maturation of the lungs, as assessed by transcriptional analyses. Time-lapse imaging reveals that branching events are synchronized across distant locations within the lung, and are preceded by long-duration waves of airway smooth muscle contraction. Higher transmural pressure decreases the interval between systemic smooth muscle contractions and increases the rate of morphogenesis of the airway epithelium. These data reveal that the mechanical properties of the microenvironment instruct crosstalk between different tissues to control the development of the embryonic lung.

KEY WORDS: Mechanical stress, Morphogenesis, Clock, Morphodynamics

INTRODUCTION

Branching morphogenesis is a common developmental program used to create complex ramified networks of epithelial tubes that support the flow of liquid or air (Warburton et al., 2010). During development of the mammalian lung, dynamic and recursive branching leads to a stereotyped airway epithelial architecture that is crucial for survival after birth (Warburton et al., 2010). Several clinical conditions result in fetal pulmonary hypoplasia, an underbranched lung, which is a major cause of respiratory insufficiency and mortality in newborns (Jobe and Ikegami, 2000; Smith et al., 2005). Pulmonary hypoplasia often co-presents with mechanical defects in the thoracic cavity, suggesting that abnormal airway branching can result from altered physical loads on the lung, even in the absence of an obvious genetic defect (Smith et al., 2005).

Much of our current understanding of the mechanisms that regulate branching morphogenesis is related to signaling pathways elucidated via genetic manipulation in small animal models (Herriges and Morrisey, 2014). Unfortunately, the small size of developing mouse lungs has rendered quantitative physical experiments intractable and, consequently, the interaction of physical mechanisms with genetic programs has not been defined. Clinical observations and studies *in vivo* of embryonic lung development in large animal models suggest a crucial role for transmural pressure, the difference between the pressure within the airway lumen and that of the pleural cavity. Experimentally decreasing transmural pressure (Fewell et al., 1983) or reducing fluid movement (Jesudason et al., 2005; Miller et al., 1993) results in underbranched airways. However, the inability to simultaneously alter the mechanical loads on the lung and observe the resulting branching dynamics has represented a critical barrier to our understanding of the mechanisms underlying relatively common fetal disorders (Warburton et al., 2010).

RESULTS AND DISCUSSION

Here, we present a microfluidic approach to precisely control the mechanical environment of the fetal lung by dynamically and quantitatively controlling the transmural pressure across intact murine embryonic lung explants (Fig. 1A). Our 'microfluidic chest cavities' consist of two separate chambers connected by a fabricated glass microneedle (Fig. 1B). Lungs dissected on embryonic day (E) 12 were intubated through the trachea with the glass microneedle and secured using a modified finger-trap suture (Fig. 1C), and then the chambers were sealed between two glass coverslips. The pleural chamber (with fluid pressure $P_{pleural}$) enclosed the explant, while the lumenal chamber (with fluid pressure P_{lumen}) accessed the airways via the intubated trachea. The pressure difference between the two chambers defined the transmural pressure ($\Delta P = P_{lumen} - P_{pleural}$) across the developing lung, morphogenesis of which was followed via time-lapse imaging for up to 78 h. In contrast to the flattened architecture observed in standard explants (Fig. S1A,B), lungs cultured within the microfluidic chest cavities developed a 3D branched architecture with distinct lobation patterns (Fig. 1D) – one lobe on the left and four lobes on the right – similar to the intact lung *in utero* (Fig. S1C-E). To characterize the resulting airway morphology, we used confocal sections of immunostained explants to create 3D reconstructions of the branched epithelium (Fig. 1E; Movie 1), followed by a skeletonization algorithm to quantify morphological parameters and the branching pattern of the airways.

As the lung develops, the airway epithelium secretes fluid into the lumen that generates a positive pressure against the closed fetal larynx (Harding and Hooper, 1996), thus producing a static or 'tonic' ΔP of ~200-400 Pa (1.5-3 mm Hg) (Olver et al., 2004; Schittny et al., 2000). Surgically occluding the trachea, which is thought to increase ΔP, has been shown to enhance branching in murine lung explants (Blewett et al., 1996; Unbekandt et al., 2008). To quantify precisely the effects of ΔP on airway architecture, we cultured explants for 48 h in the microfluidic chest cavities over a range of ΔP spanning those

[1]Department of Chemical & Biological Engineering, Princeton University, Princeton, NJ 08544, USA. [2]Molecular Biology, Princeton University, Princeton, NJ 08544, USA. [3]Quantitative and Computational Biology, Princeton University, Princeton, NJ 08544, USA. [4]Department of Cancer Biology, Mayo Clinic Cancer Center, Jacksonville, FL 32224, USA. [5]Mechanical and Aerospace Engineering, Princeton University, Princeton, NJ 08544, USA.
*Present address: Department of Biomedical Engineering, University of Delaware, Newark, DE 19726, USA.
‡These authors contributed equally to this work

§Author for correspondence (celesten@princeton.edu)

C.M.N., 0000-0001-9973-8870

Received 15 May 2017; Accepted 24 October 2017

Development (2017) 144, 4328-4335 doi:10.1242/dev.154823

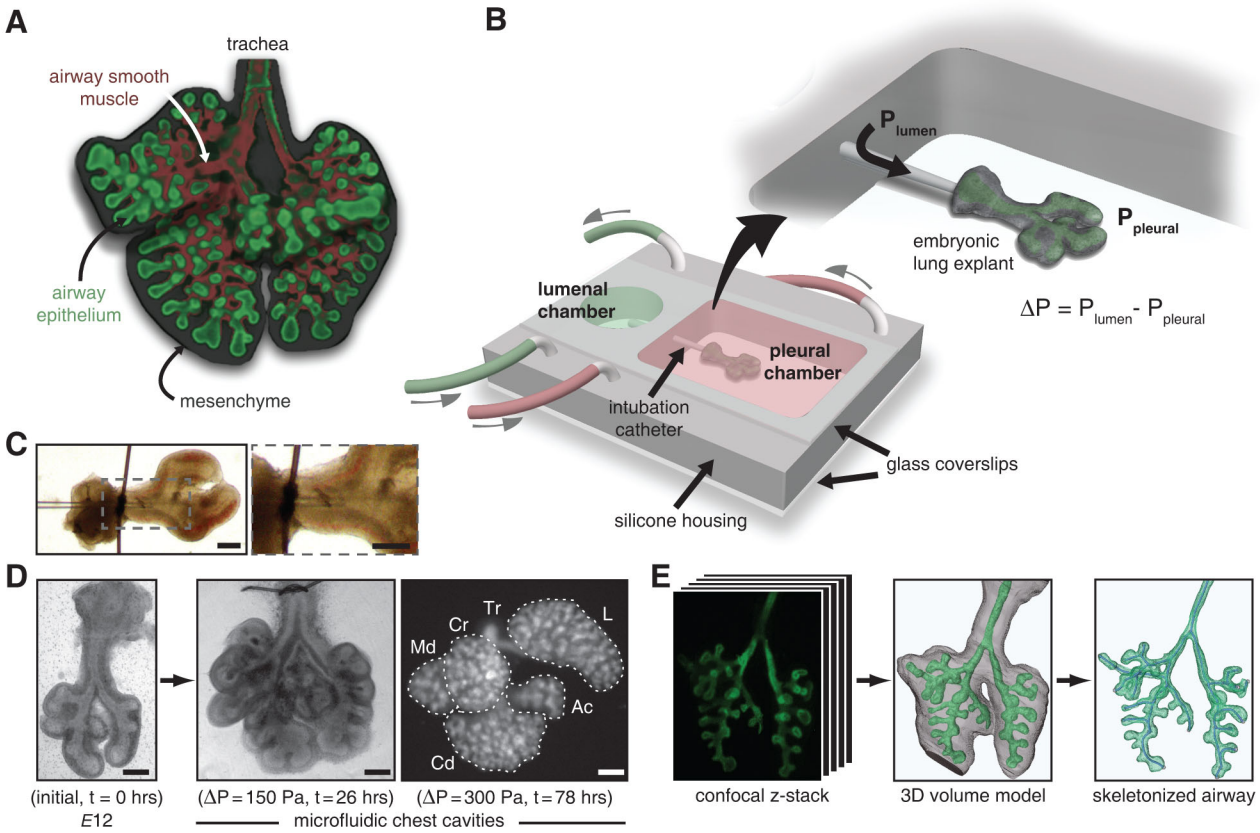

Fig. 1. Morphogenesis of embryonic murine lung explants cultured in 'microfluidic chest cavities'. (A) Architecture of the developing mouse lung. The airway epithelial tree (green) is surrounded by mesenchyme (gray). Airway smooth muscle (red) wraps around the proximal epithelial branches. (B,C) Microfluidic chest cavities consisted of one chamber in which the organ was cultured (pleural chamber) and a second chamber that accessed the airways of the lung (lumenal chamber) (B) through the intubated trachea (C). (D) Lung explants cultured in the microfluidic chest cavities developed a 3D branched architecture with five lobes as *in vivo*. Ac, accessory lobe; Cd, caudal lobe; Cr, cranial lobe; L, left lobe; Md, middle lobe; Tr, trachea. (E) Airway architecture was reconstructed from high-resolution confocal *z*-stacks and the resulting 3D volume model was skeletonized. Scale bars: 100 µm in C; 250 µm in D.

observed during normal (Harding and Hooper, 1996) and pathologic (Kitterman, 1996) development *in vivo*, and under standard culture *ex vivo* (Fig. 2A). We found that lung development occurred in a pressure-dependent manner, with higher ΔP leading to increased growth of the epithelium and mesenchyme, as well as commensurate increases in the overall size of the organ and architectural complexity of the airways. The number of terminal branches increased as ΔP increased (Fig. 2B), consistent with qualitative observations from tracheal occlusion studies.

These pressure-mediated changes in airway architecture could arise from two different mechanisms. Transmural pressure could increase the number of branches by stochastically altering the topology of the epithelial tree (i.e. changing the pattern of branching), or it could increase the rate at which a conserved airway topology elaborates over time. To distinguish between these two possibilities, we quantified the topology of the airway epithelial tree after 48 h at each ΔP by constructing lineage diagrams from our skeletonized 3D reconstructions, using anatomical nomenclature reported previously (Metzger et al., 2008) (Fig. 2C; Fig. S2). This analysis revealed that the branching pattern of the airways remained remarkably stereotyped, consistent with that of lungs isolated from embryos later in gestation. Lungs cultured at lower ΔP were less mature overall and generated a subset of the branches that formed in explants at higher pressures. These data show that ΔP controls the rate, but not the pattern, of airway epithelial branching.

Gene expression profiling supported this conclusion. We conducted RNA sequencing (RNA-Seq) analysis on lungs held for 48 h at low (20 Pa) or high (300 Pa) ΔP, as well as those isolated directly from embryos on E12.5, E13.5 and E14.5. We then analyzed genes that were differentially expressed ($P<0.05$) between E14.5 and E12.5 (2095 genes), and between high and low ΔP (2237 genes), using the NextBio platform (Kupershmidt et al., 2010), and found significant overlap between the two ($P=5.5\times10^{-72}$; Fig. 2D); of these overlapping genes, the majority changed in the same direction in both data sets ($P=3.3\times10^{-90}$ increased, $P=1.1\times10^{-78}$ decreased; Fig. 2E). However, because many genes did not overlap, we performed a principal component analysis (PCA) to better understand these differences (Fig. S3A). Not surprisingly, PCA revealed that key differences in gene expression resulted from comparing lungs held in culture to those isolated directly from the embryo (Fig. S3B,C). Nonetheless, PCA of both the full data set and the 500 most-variable genes showed that the high ΔP and E14.5 lungs clustered separately from the remaining samples (Fig. 2F; Fig. S3D-F), consistent with our topology analysis.

These data suggest that ΔP drives expression of lung developmental gene programs. Gene Ontology analysis showed regulation of transcripts associated with morphogenesis, development, cell motility and migration, and extracellular matrix in both groups (Fig. S3G). RT-PCR analysis confirmed that high ΔP enhances the expression of genes that drive airway branching morphogenesis, such as fibroblast growth factors (FGFs) (Fig. S4A-D). High ΔP also

Development (2017) 144, 4328-4335 doi:10.1242/dev.154823

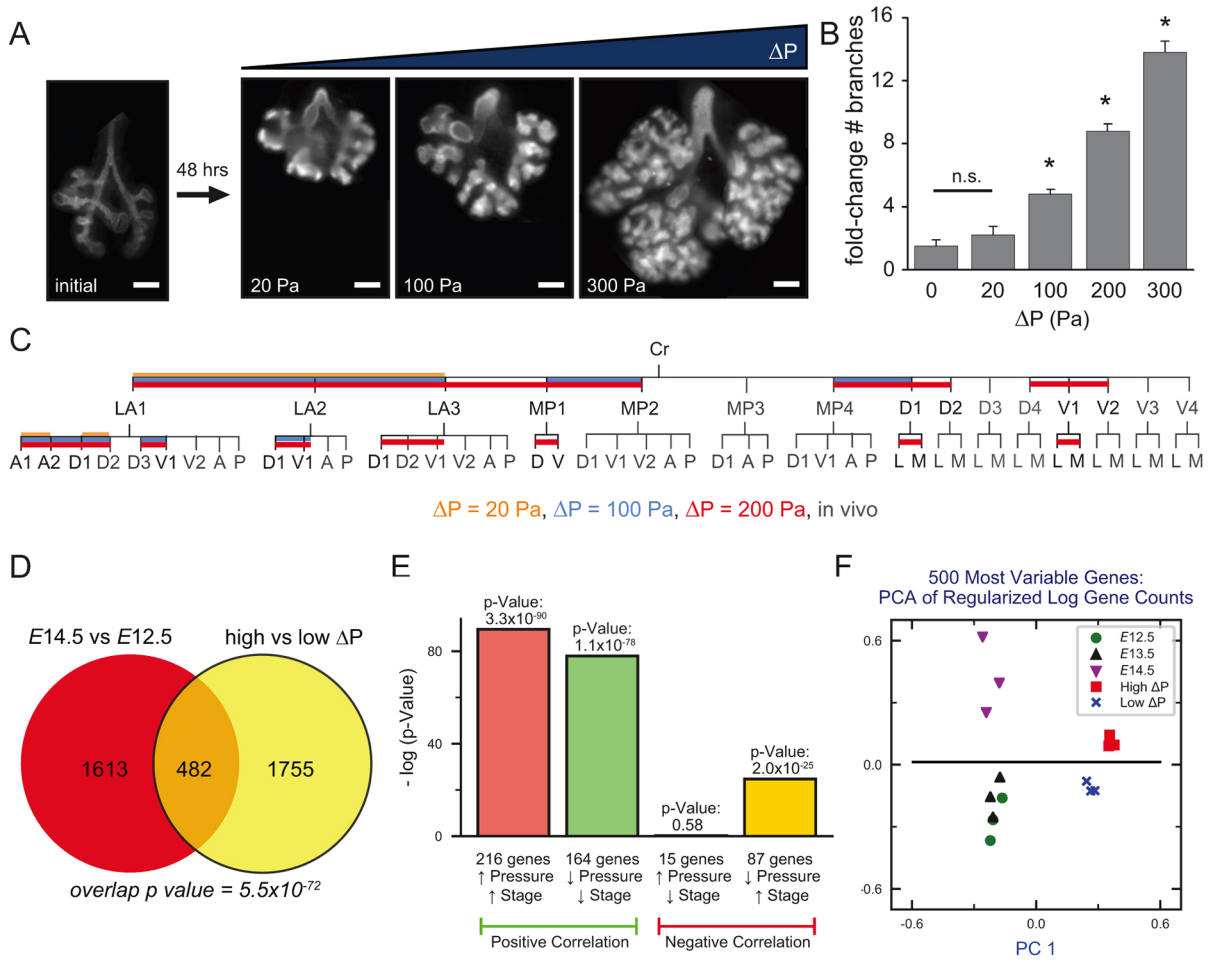

Fig. 2. Transmural pressure regulates the rate at which the airway epithelium branches without affecting the stereotyped branching pattern. (A) Lung explants cultured at different ΔP immunostained for E-cadherin. Scale bars: 200 µm. (B) Quantification of the change in number of branches as a function of ΔP. Data are mean±s.d. for at least five replicates; *P<0.05; n.s., not significant, as compared to 0 Pa condition (one-way ANOVA). (C) Lineage diagrams of the branches within the cranial lobe (Cr) of three representative explants cultured under different ΔP (orange, 20 Pa; blue, 100 Pa; red, 200 Pa) overlaid on a partial lineage diagram for an E14 explant (gray, *in vivo*). Fully annotated lineage diagrams can be found in Fig. S2. (D) Venn diagram showing overlap in genes that are differentially expressed at E14.5 versus E12.5 and under high versus low ΔP. (E) Overlap of genes that are positively or negatively correlated between data sets among the 482 genes that overlap in D. (F) The first two principal components of each RNA-Seq biological replicate using the 500 genes with the highest variances (each biological replicate represents RNA pooled from three to six lungs). The horizontal line illustrates how E14.5 and high ΔP lungs separate from E12.5, E13.5 and low ΔP lungs along the second principal component.

enhances the expression of genes involved with airway maturation, including surfactant proteins and mucin (Fig. S4E-J). Collectively, our data suggest that lungs held at higher ΔP are more developmentally mature than those held at lower pressures.

To characterize how ΔP affects the kinematics of morphogenesis, we used time-lapse imaging of lungs cultured within the microfluidic chest cavities to quantify branching dynamics. Tracing the projected area of the epithelium over time (Fig. 3A) allowed us to annotate lineage diagrams with the time at which branches formed (Fig. 3B). These temporal lineage studies surprisingly revealed that branching occurred synchronously approximately every 10 h for lungs held at a ΔP of 300 Pa (Fig. 3C); that is, branches formed simultaneously (within ±10 min of each other) at distant locations throughout the epithelial tree (Fig. 3D). The timing between these synchronized bursts of branching was pressure dependent (Fig. 3E), with higher ΔP decreasing the interval (Δt) between bursts.

This demonstration of periodic synchronized branching emphasizes the fact that morphogenesis of the airway epithelium is regulated globally within the lung. As the lung develops, smooth muscle encircles the airways and helps guide branch sites (Kim et al., 2015) (Fig. S5A,B). In cultured explants, nonuniform peristalsis-like contractions of the proximal airway smooth muscle have been observed to move fluid throughout the lumen, causing the tips of distal branches to cyclically dilate and relax (Schittny et al., 2000). To visualize the interaction of the airway epithelium and surrounding smooth muscle, we explanted lungs from transgenic mouse embryos expressing red fluorescent protein under the control of the α-smooth muscle actin promoter (αSMA-RFP) (Magness et al., 2004) (Fig. S5C). In addition to periodic high-frequency (~1 min^{-1}) peristalsis-like contractions (Fig. S5D), we also observed longer timescale systemic smooth muscle contractions, which caused a net flux of fluid into the extending branches (Fig. 3F; Movie 2), and gradually decreased the diameter of the proximal airways throughout the epithelial tree (Fig. 3G). These systemic contractions (dashed red lines in Fig. 3B) began 6-12 min before new branches appeared, continued as the branches extended, and were regulated by ΔP (Fig. 3E). Pharmacologically inhibiting smooth muscle contraction with nifedipine (Movie 3) (Kim et al.,

Development (2017) 144, 4328-4335 doi:10.1242/dev.154823

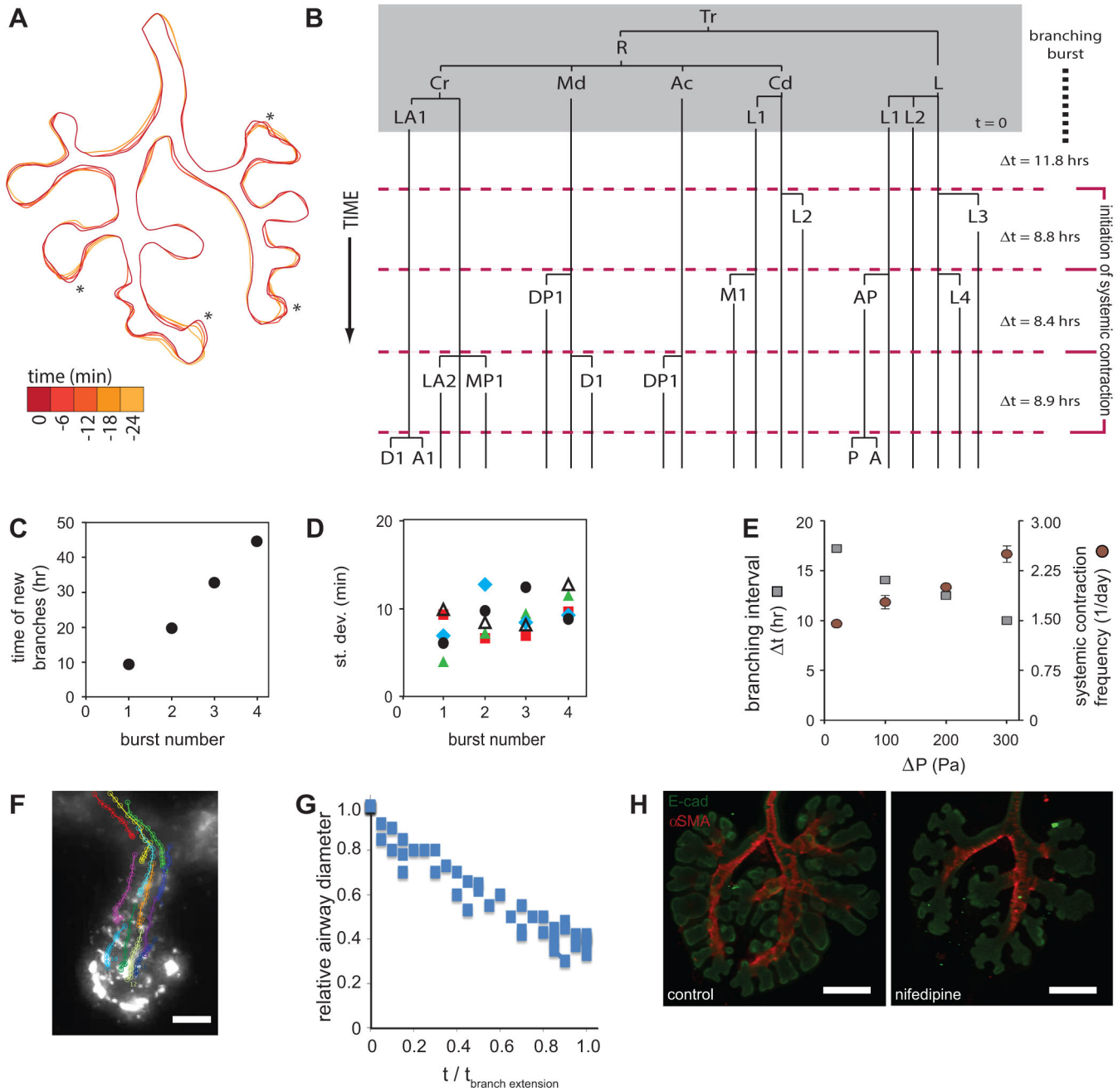

Fig. 3. Transmural pressure regulates the timing of synchronized branching and the rate of systemic smooth muscle contraction. (A) Tracings of the epithelial perimeter over time reveal that branches (asterisks) form simultaneously. (B) Temporal lineage diagram reveals that new branches emerge simultaneously in different regions of the epithelial tree. Vertical lines indicate the hierarchical relationship between branches, and the position of the branch node indicates the time of branch initiation. Systemic contractions of airway smooth muscle (red dashed line) occur immediately prior to epithelial branching. Panel A shows the second burst of branching of the lung in B, which was held at ΔP=300 Pa. (C,D) The time at which new branches form during each burst of branching after the start of culture (C) and the standard deviation of branch formation (D) within each burst for five different explants, for lungs held at ΔP=300 Pa. (E) The interval between epithelial branching (Δt) and frequency of systemic smooth muscle contraction depend on ΔP. Data are mean±s.d. for at least six explants. (F,G) As a branch forms and extends, systemic contractions drive lumenal fluid to the distal tips, as visualized by different colored pathlines from individually tracked fluorescent fluid tracers (F), and the lumenal diameter of the proximal airway decreases (G). (H) Pharmacologically inhibiting airway smooth muscle contraction arrests branching and lung development. Scale bars: 50 µm in F; 300 µm in H.

2015), an L-type calcium channel blocker, disrupted systemic contractions and arrested branch extension (Fig. 3H). These results suggest that ΔP regulates both the timing of airway branching and of systemic smooth muscle contractions, which may be coupled globally across the lung. Although systemic contractions occurred periodically, and branches formed with each contraction, not every generation branched with each contraction.

In congenital diaphragmatic hernia, the herniation of abdominal organs is often confined to one side of the chest cavity, resulting in airway hypoplasia localized to that side. These observations suggest that physical boundary conditions might play a role in locally defining ΔP. To distinguish between effects caused by lumenal pressure and those caused by spatial constraints, we held P_{lumen} constant while constraining one lobe of the lung under hydrogel

Development (2017) 144, 4328-4335 doi:10.1242/dev.154823

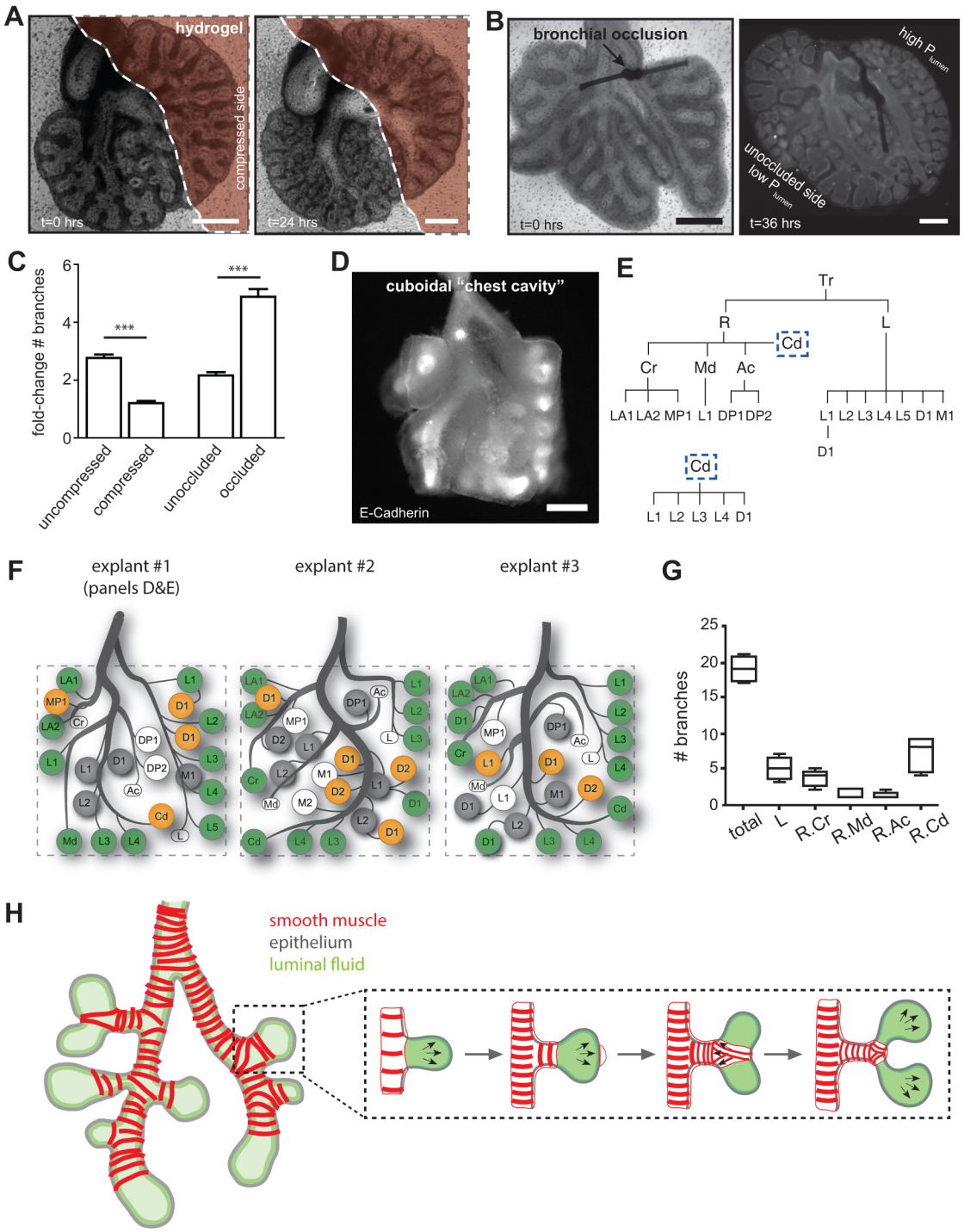

Fig. 4. Local transmural pressure alters proximal smooth muscle contraction and tunes airway branching. (A-C) Differential ΔP achieved in cultured explants by modulating $P_{pleural}$ by compressing half of the explant under collagen gel (A) or modulating P_{lumen} using bronchial ligation (B) unilaterally alters the extent of branching (C). As such, the physical boundary conditions placed on the developing organ can locally modulate ΔP and sculpt airway architecture. Data are mean±s.d. for four replicates; ***P<0.001 (Student's t-test). (D,E) Explants cultured in cuboidal microfluidic chest cavities (600 µm per side) formed a gross morphology that matches the shape of the chamber (D), with a corresponding lineage diagram (E). Branch names from Metzger et al. (2008). (F) Schematic diagrams of airways that formed in three different explants cultured within cuboidal microfluidic chest cavities. (G) The number of branches that form in the whole lung (total) and in each lobe in cuboidal chest cavities. Box shows median and interquartile range. Whiskers show maximum and minimum. (H) Transmural pressure from luminal fluid (green) enhances the expansion of the airway epithelium (gray) and differentiation of airway smooth muscle (red); contraction of the airway smooth muscle precedes (and likely patterns) epithelial branching. Scale bars: 150 µm.

(Fig. 4A), decreasing ΔP. As a comparison, we ligated the primary bronchi of lungs cultured within our microfluidic chest cavities to asymmetrically increase ΔP in the occluded bronchus (Fig. 4B). In both cases, physically constraining ΔP on one side of the developing lung resulted in different extents of branching within the same explant (Fig. 4C). At later stages of development, the individual lobes of the lung interlock (Fig. S1C) and the organ conforms to the contours of the thoracic cavity, despite the absence of structural

Development (2017) 144, 4328-4335 doi:10.1242/dev.154823

connections between the lung and the chest wall. In the relatively spacious microfluidic chest cavity, the explants developed the stereotyped lobation pattern, but the gross geometry of the lobes was rounded and noninterlocking. To determine whether ΔP and physical boundary conditions might regulate the global architecture of the lung, we cultured explants in microfluidic chest cavities of defined shapes. The final overall geometry of these explants conformed to the shape of the microfluidic chamber, generating cuboidal (Fig. 4D), cylindrical, triangular or rectangular-prism-shaped organs (Fig. S6), with branches (Fig. 4E) that formed interlocking lobes. Branching morphogenesis of each lobe halted once the daughter branches contacted the walls of the microfluidic chest cavity (Fig. 4F). For cuboidal chest cavities, lungs formed 19±1 terminal branches before morphogenesis stopped (Fig. 4G), consistent with a space-filling program.

These data reveal that development of the airway epithelium and its surrounding mesenchyme are controlled by the relative pressure of the fluid contained within the lumen of the lung (Fig. 4H). Although other studies have identified key molecular and genetic mediators of airway stereotypy (Metzger et al., 2008; Morrisey and Hogan, 2010), our data suggest that airway branching morphogenesis is not driven solely by a closed genetic program but is also controlled by mechanical cues, consistent with an increasing appreciation for mechanical forces in the morphogenesis of a wide variety of tissues (Desprat et al., 2008; Hutson et al., 2003; Martin et al., 2009; Nelson and Gleghorn, 2012; Nerurkar et al., 2006; Varner et al., 2010). We have shown that ΔP regulates the rate and timing of epithelial branching, and that branching events are synchronized throughout the developing airway tree. Importantly, ΔP regulates both the timing of branching morphogenesis and the frequency of systemic contractions of airway smooth muscle. These results reveal the existence of a pressure-dependent mechanical 'clock' that coordinates morphogenesis at distant sites within the developing organ to control and synchronize branching events within the airway epithelium. Thus, the functional behavior of one developing tissue (the contraction of smooth muscle) is connected to the morphogenesis of an adjacent tissue (the branching of the epithelium). It will be interesting to determine the molecular and physical connections between systemic smooth muscle contraction and synchronized epithelial branching in the future.

The function of airway smooth muscle has been controversial (Fredberg, 2007; Mead, 2007; Mitzner, 2004) and most often investigated in the context of postnatal diseases such as asthma (Janssen and Killian, 2006). Our findings suggest the possibility of a specific and unappreciated instructional role for airway smooth muscle during early lung development. The timing of systemic contractions of airway smooth muscle and formation of epithelial branches are linked, and both are regulated by ΔP. Although the underlying molecular mechanism is unclear, mechanical stretch has been found to regulate the contractile phenotype of vascular smooth muscle cells (Stegemann et al., 2005), and similar signaling could be at work in the developing lung. Indeed, overexpressing *Cftr* was found to both increase luminal fluid secretion and enhance the expression of smooth muscle-specific proteins in the embryonic rat lung (Cohen and Larson, 2006). Our data suggest that increasing the frequency of smooth muscle contraction might normalize airway development in fetuses suffering from conditions that usually result in airway hypoplasia.

Organ development is currently considered to be a genetically driven process, in part because the experimental tools used to investigate morphogenesis have been genetic in nature. Our study shows that mechanical tools, such as those presented here, can reveal the nongenetic physical mechanisms that also regulate development. Here, we have shown that a microenvironmental factor (fluid pressure) can quantitatively regulate the rate of morphogenesis. It is possible that pressure-mediated control of morphogenesis is a conserved regulatory mechanism across different organs and species, as other studies have suggested that fluid pressure might drive expansion of the chicken neural tube (Desmond and Jacobson, 1977), *Drosophila* trachea (Tsarouhas et al., 2007) and zebrafish Kupffer's vesicle (Navis et al., 2013). The ability to regulate the mechanical microenvironment of developing organs offers a powerful vertebrate model to study morphogenesis, mimic common fetal diseases, and parse the interactions between molecular and physical mechanisms of development.

MATERIALS AND METHODS

Isolation and culture of lung explants

Embryos were isolated from euthanized timed-pregnant mice (*Mus musculus*, CD-1) at E12.5 and stored in chilled phosphate-buffered saline (PBS) prior to dissection. Transgenic embryos expressing αSMA-RFP (Kim et al., 2015) were similarly isolated and stored. All experiments complied with ethical regulations for the care and use of animals, as approved by the Princeton University Institutional Animal Care and Use Committee. Sample size was determined by estimating the variance in preliminary experiments, with a power analysis for a power of 0.8. Lungs were dissected following standard protocols in chilled PBS supplemented with 10 U/ml penicillin and 10 µg/ml streptomycin (Sigma-Aldrich), taking care to extract the entire length of the trachea. Explants were either cultured in the microfluidic chest cavities or at the air-fluid interface on floating rafts (Schittny et al., 2000) in DMEM:F12 medium (HyClone) supplemented with 5% fetal bovine serum (Atlanta Biologicals), 10 U/ml penicillin and 10 µg/ml streptomycin. To pharmacologically inhibit airway smooth muscle contraction, nifedipine (10 µM; Sigma-Aldrich) was added to the culture medium for the duration of the experiment. For time-lapse analysis, explants were cultured within the microfluidic chest cavities at 37°C and 5% CO_2 in a humidified stage-top incubator. Brightfield and/or fluorescence images were acquired every 6 min for the duration of the culture period.

Design and fabrication of microfluidic chest cavities

Microfluidic devices consisted of a layer of micromolded polydimethylsiloxane (PDMS) bonded between two glass coverslips for structural support and optical clarity. Standard photolithographic techniques were used to generate a 100 µm thick SU-8 silicon master consisting of the two chambers and fluidic channels. PDMS was replica molded from these masters and a circular biopsy punch (8 mm diameter) was used to create the chambers in the 4 mm thick PDMS. A second biopsy punch (1 mm diameter) was used to connect the two chambers. A pulled glass catheter was inserted through the hole between the two chambers and the catheter was trimmed to length. A glass coverslip and the PDMS/catheter assembly were bonded together following treatment in a plasma cleaner. The fluidic channels, chambers and glass catheter were wetted with culture medium and bubbles were cleared from the system. A lung explant was inserted into the pleural chamber and intubated with the catheter, and the trachea was then affixed to the catheter with a modified finger-trap suture. A second plasma-cleaned glass coverslip was bonded to the roof of the chambers. The fluidic channels enabled dynamic control of the pressure within the two chambers, thus permitting application of either a constant or variable ΔP. Pressure was controlled hydrostatically by altering the height of the column of fluid above each chamber. Every 18 h, two thirds of the culture medium was replaced with fresh medium.

To alter the shape of the chest cavity, a square, circular, triangular or rectangular hole was punched into a 200 µm thick sheet of PDMS. The punched sheet was inserted into the pleural chamber of the microfluidic chest cavities prior to insertion and intubation of the lung explants, which were cultured at ΔP=200 Pa for 48 h.

Morphometric analysis

Explants were fixed in 4% paraformaldehyde in PBS for 15 min at room temperature. To visualize the airway epithelium, samples were labeled using

Development (2017) 144, 4328-4335 doi:10.1242/dev.154823

anti-E-cadherin monoclonal antibody (Invitrogen, 1:200) and Alexa Fluor 488-conjugated secondary antibody (Invitrogen, 1:200). High-resolution confocal stacks (z=2 µm) were acquired of the immunostained explants, and these data were reconstructed to create 3D volume models of the epithelial tree using Amira (FEI Visualization Sciences Group). Briefly, the 3D image data were segmented and fit to an isosurface to define a 3D object. A skeletonization algorithm was then applied to the model of the airways to define the centerlines and connection points of all branches. We used this framework to quantify and compare the branching pattern, hierarchy and aspect ratio of the airways. To compare the effects of different ΔP, we quantified the branching hierarchy of at least four explants per pressure condition per experiment; experiments were conducted independently using embryos from at least three different mothers to permit conclusions about stereotypy.

For time-lapse experiments, morphometric analysis was conducted using 2D maximum intensity projections of brightfield and fluorescence images. To quantify branch contraction, we measured the diameter of the airway halfway along the length of the proximal branches as a function of time. Measurements of ≥20 branching events from seven different explants were used to construct lineage diagrams (Fig. 3B-E). Because the pattern of branching in the mouse lung is stereotyped, the locations of daughter branches are known in advance; the time at which they emerged was determined by measuring when the epithelium at the site of a new branch deformed by ≥15 µm (~20% of the mean luminal diameter) relative to the surrounding airway.

Tracking flow of luminal fluid

Fluorescent polystyrene microspheres (0.5 µm diameter, Invitrogen) were microinjected into the lumens of five freshly isolated lung explants. Explants were cultured in the microfluidic chest cavities and imaged over time to track the movements of the beads within the luminal fluid. Particle tracking was performed using ImageJ (https://imagej.nih.gov/ij/).

Gene expression analysis

Gene expression analysis was carried out on lungs at stages E12.5, E13.5 and E14.5, as well as lung explants cultured at either 20 Pa (low ΔP) or 300 Pa (high ΔP) for 48 h. Tissue from several lungs was homogenized using QIAshredder (Qiagen) columns. RNA from the resulting sample was purified using the RNEasy Fibrous Tissue Mini Kit (Qiagen) and cDNA was synthesized using the Verso cDNA synthesis kit (Thermo Fisher Scientific). For RNA-Seq, the quality of total RNA was assessed by RNA 6000 Nanochip using an Agilent Bioanalyzer. The cDNA libraries were constructed using polyA-enriched RNA according to the manufacturer's instructions (Illumina). Sequencing was performed at the Lewis Sigler Institute for Integrative Genomics sequencing core facility using the Illumina HiSeq 2000 Platform. Reads were mapped to transcripts using TopHat (Trapnell et al., 2009) and gene counts were identified by HTSeq-count (Anders et al., 2015). Differentially expressed genes were identified using DEseq2 (Love et al., 2014), which employs a statistical model to handle low-expressing genes by shrinking their estimated log-fold changes to avoid false-positive P values. PCA was completed on these statistically normalized data using Python. Instead of choosing a cutoff for magnitude of relative expression, genes were considered to be differentially expressed if their P value, adjusted for multiple testing by the Benjamini–Hochberg procedure, was <0.05. A total of 2113 genes were selected as differentially expressed between E14.5 and E12.5 lung samples, and 2259 genes were selected as differentially expressed between explants held at high and low ΔP; these matched 2095 and 2337 features, respectively, in the Nextbio database (Kupershmidt et al., 2010), which was used for gene set overlap and Gene Ontology analysis as described previously (Cichon et al., 2015). The Nextbio server uses the 2012-10-10 data version of Gene Ontology annotations.

For quantitative PCR analysis, cDNA was synthesized using the Verso cDNA synthesis kit (Thermo Fisher Scientific). Quantitative RT-PCR was performed on a StepOnePlus real-time PCR system (Applied Biosystems) using iTaq SYBR green supermix (BioRad) and the primers indicated in Table S1. Primer pairs were designed using Primer-BLAST (NCBI) software (Ye et al., 2012). Expression levels for each transcript were normalized to that of 18S rRNA in each sample.

Acknowledgements

We thank the Lewis-Sigler Institute for Integrative Genomics Sequencing Core Facility for RNA sequencing and Lance Parsons for assistance with data analysis.

Competing interests

The authors declare no competing or financial interests.

Author contributions

Conceptualization: C.M.N., J.P.G., H.A.S.; Methodology: C.M.N., J.P.G., M.-F.P., J.M.J.; Formal analysis: C.M.N., J.M.J.; Investigation: J.P.G., M.-F.P., K.G., V.D.V.; Resources: E.M., D.C.R.; Writing - original draft: J.P.G.; Writing - review & editing: C.M.N., M.-F.P., J.M.J., D.C.R.; Supervision: C.M.N.; Project administration: C.M.N.; Funding acquisition: C.M.N.

Funding

This work was supported by the National Institutes of Health [GM083997, HL110335, HL118532 and HL120142], the Division of Civil, Mechanical and Manufacturing Innovation [CMMI-1435853], the David and Lucile Packard Foundation, the Alfred P. Sloan Foundation, the Camille and Henry Dreyfus Foundation, and the Burroughs Wellcome Fund. M.-F.P. was supported, in part, by postdoctoral fellowships from Svenska Sällskapet för Medicinsk Forskning and the New Jersey Commission on Cancer Research. J.P.G. was supported, in part, by a Basil O'Connor Starter Scholar Award from the March of Dimes Foundation. CMN was supported, in part, by a Faculty Scholars Award from the Howard Hughes Medical Institute. Deposited in PMC for release after 12 months.

Data availability

RNA-Seq data that support the findings of this study have been deposited in Gene Expression Omnibus with the GEO accession GSE90148.

Supplementary information

Supplementary information available online at
http://dev.biologists.org/lookup/doi/10.1242/dev.154823.supplemental

References

Anders, S., Pyl, P. T. and Huber, W. (2015). HTSeq–a Python framework to work with high-throughput sequencing data. *Bioinformatics* **31**, 166-169.

Blewett, C. J., Zgleszewski, S. E., Chinoy, M. R., Krummel, T. M. and Cilley, R. E. (1996). Bronchial ligation enhances murine fetal lung development in whole-organ culture. *J. Pediatr. Surg.* **31**, 869-877.

Cichon, M. A., Nelson, C. M. and Radisky, D. C. (2015). Regulation of epithelial-mesenchymal transition in breast cancer cells by cell contact and adhesion. *Cancer Inform.* **14**, 1-13.

Cohen, J. C. and Larson, J. E. (2006). Cystic fibrosis transmembrane conductance regulator (CFTR) dependent cytoskeletal tension during lung organogenesis. *Dev. Dyn.* **235**, 2736-2748.

Desmond, M. E. and Jacobson, A. G. (1977). Embryonic brain enlargement requires cerebrospinal fluid pressure. *Dev. Biol.* **57**, 188-198.

Desprat, N., Supatto, W., Pouille, P.-A., Beaurepaire, E. and Farge, E. (2008). Tissue deformation modulates twist expression to determine anterior midgut differentiation in Drosophila embryos. *Dev. Cell* **15**, 470-477.

Fewell, J. E., Hislop, A. A., Kitterman, J. A. and Johnson, P. (1983). Effect of tracheostomy on lung development in fetal lambs. *J. Appl. Physiol.* **55**, 1103-1108.

Fredberg, J. J. (2007). Counterpoint: airway smooth muscle is not useful. *J. Appl. Physiol. (1985)* **102**, 1709-1710; discussion 1710-1701.

Harding, R. and Hooper, S. B. (1996). Regulation of lung expansion and lung growth before birth. *J. Appl. Physiol.* **81**, 209-224.

Herriges, M. and Morrisey, E. E. (2014). Lung development: orchestrating the generation and regeneration of a complex organ. *Development* **141**, 502-513.

Hutson, M. S., Tokutake, Y., Chang, M. S., Bloor, J. W., Venakides, S., Kiehart, D. P. and Edwards, G. S. (2003). Forces for morphogenesis investigated with laser microsurgery and quantitative modeling. *Science* **300**, 145-149.

Janssen, L. J. and Killian, K. (2006). Airway smooth muscle as a target of asthma therapy: history and new directions. *Respir. Res.* **7**, 123.

Jesudason, E. C., Smith, N. P., Connell, M. G., Spiller, D. G., White, M. R. H., Fernig, D. G. and Losty, P. D. (2005). Developing rat lung has a sided pacemaker region for morphogenesis-related airway peristalsis. *Am. J. Respir. Cell Mol. Biol.* **32**, 118-127.

Jobe, A. H. and Ikegami, M. (2000). Lung development and function in preterm infants in the surfactant treatment era. *Annu. Rev. Physiol.* **62**, 825-846.

Kim, H. Y., Pang, M.-F., Varner, V. D., Kojima, L., Miller, E., Radisky, D. C. and Nelson, C. M. (2015). Localized smooth muscle differentiation is essential for epithelial bifurcation during branching morphogenesis of the mammalian lung. *Dev. Cell* **34**, 719-726.

Kitterman, J. A. (1996). The effects of mechanical forces on fetal lung growth. *Clin. Perinatol.* **23**, 727-740.

Kupershmidt, I., Su, Q. J., Grewal, A., Sundaresh, S., Halperin, I., Flynn, J., Shekar, M., Wang, H., Park, J., Cui, W. et al. (2010). Ontology-based meta-analysis of global collections of high-throughput public data. *PLoS ONE* **5**, e13066.

Love, M. I., Huber, W. and Anders, S. (2014). Moderated estimation of fold change and dispersion for RNA-seq data with DESeq2. *Genome Biol.* **15**, 550.

Magness, S. T., Bataller, R., Yang, L. and Brenner, D. A. (2004). A dual reporter gene transgenic mouse demonstrates heterogeneity in hepatic fibrogenic cell populations. *Hepatology* **40**, 1151-1159.

Martin, A. C., Kaschube, M. and Wieschaus, E. F. (2009). Pulsed contractions of an actin-myosin network drive apical constriction. *Nature* **457**, 495-499.

Mead, J. (2007). Point: airway smooth muscle is useful. *J. Appl. Physiol. (1985)* **102**, 1708-1709; discussion 1710.

Metzger, R. J., Klein, O. D., Martin, G. R. and Krasnow, M. A. (2008). The branching programme of mouse lung development. *Nature* **453**, 745-750.

Miller, A. A., Hooper, S. B. and Harding, R. (1993). Role of fetal breathing movements in control of fetal lung distension. *J. Appl. Physiol.* **75**, 2711-2717.

Mitzner, W. (2004). Airway smooth muscle: the appendix of the lung. *Am. J. Respir. Crit. Care. Med.* **169**, 787-790.

Morrisey, E. E. and Hogan, B. L. M. (2010). Preparing for the first breath: genetic and cellular mechanisms in lung development. *Dev. Cell* **18**, 8-23.

Navis, A., Marjoram, L. and Bagnat, M. (2013). Cftr controls lumen expansion and function of Kupffer's vesicle in zebrafish. *Development* **140**, 1703-1712.

Nelson, C. M. and Gleghorn, J. P. (2012). Sculpting organs: mechanical regulation of tissue development. *Annu. Rev. Biomed. Eng.* **14**, 129-154.

Nerurkar, N. L., Ramasubramanian, A. and Taber, L. A. (2006). Morphogenetic adaptation of the looping embryonic heart to altered mechanical loads. *Dev. Dyn.* **235**, 1822-1829.

Olver, R. E., Walters, D. V. and Wilson, S. M. (2004). Developmental regulation of lung liquid transport. *Annu. Rev. Physiol.* **66**, 77-101.

Schittny, J. C., Miserocchi, G. and Sparrow, M. P. (2000). Spontaneous peristaltic airway contractions propel lung liquid through the bronchial tree of intact and fetal lung explants. *Am. J. Respir. Cell Mol. Biol.* **23**, 11-18.

Smith, N. P., Jesudason, E. C., Featherstone, N. C., Corbett, H. J. and Losty, P. D. (2005). Recent advances in congenital diaphragmatic hernia. *Arch. Dis. Child.* **90**, 426-428.

Stegemann, J. P., Hong, H. and Nerem, R. M. (2005). Mechanical, biochemical, and extracellular matrix effects on vascular smooth muscle cell phenotype. *J. Appl. Physiol.* **98**, 2321-2327.

Trapnell, C., Pachter, L. and Salzberg, S. L. (2009). TopHat: discovering splice junctions with RNA-Seq. *Bioinformatics* **25**, 1105-1111.

Tsarouhas, V., Senti, K.-A., Jayaram, S. A., Tiklova, K., Hemphala, J., Adler, J. and Samakovlis, C. (2007). Sequential pulses of apical epithelial secretion and endocytosis drive airway maturation in Drosophila. *Dev. Cell* **13**, 214-225.

Unbekandt, M., del Moral, P.-M., Sala, F. G., Bellusci, S., Warburton, D. and Fleury, V. (2008). Tracheal occlusion increases the rate of epithelial branching of embryonic mouse lung via the FGF10-FGFR2b-Sprouty2 pathway. *Mech. Dev.* **125**, 314-324.

Varner, V. D., Voronov, D. A. and Taber, L. A. (2010). Mechanics of head fold formation: investigating tissue-level forces during early development. *Development* **137**, 3801-3811.

Warburton, D., El-Hashash, A., Carraro, G., Tiozzo, C., Sala, F., Rogers, O., De Langhe, S., Kemp, P. J., Riccardi, D., Torday, J. et al. (2010). Lung organogenesis. *Curr. Top. Dev. Biol.* **90**, 73-158.

Ye, J., Coulouris, G., Zaretskaya, I., Cutcutache, I., Rozen, S. and Madden, T. L. (2012). Primer-BLAST: a tool to design target-specific primers for polymerase chain reaction. *BMC Bioinformatics* **13**, 134.

Supplemental Material

Supplemental Table

Gene	Primer Sequences
fgf7	Forward: 5'-GCAATCAAAGGGGTGGAAAGTG-3' Reverse: 5'-TCCATTTAGCTGATGCATAGGTG-3'
fgf10	Forward: 5'-ACTTAGCCATGAACAAGAAGGG-3' Reverse: 5'-TTTGCCTGCCATTGTGCTG-3'
sfta2	Forward: 5'- CTGCCATCAGGGACCAATGT-3' Reverse: 5'- AAGGCGTGTTCACTTCCCAA-3'
sftpc	Forward: 5'- GGAGCACCGGAAACTCAGAA -3' Reverse: 5'- CTGGCTTATAGGCCGTCAGG -3'
muc1	Forward: 5'- CCAAGCGTAGCCCCTATGAG -3' Reverse: 5'- GTGGGGTGACTTGCTCCTAC -3'
18S	Forward: 5'- TCAGATACCGTCGTAGTTC -3' Reverse: 5'- CCTTTAAGTTTCAGCTTTGC -3'

Development • Supplementary information

Supplemental Movies

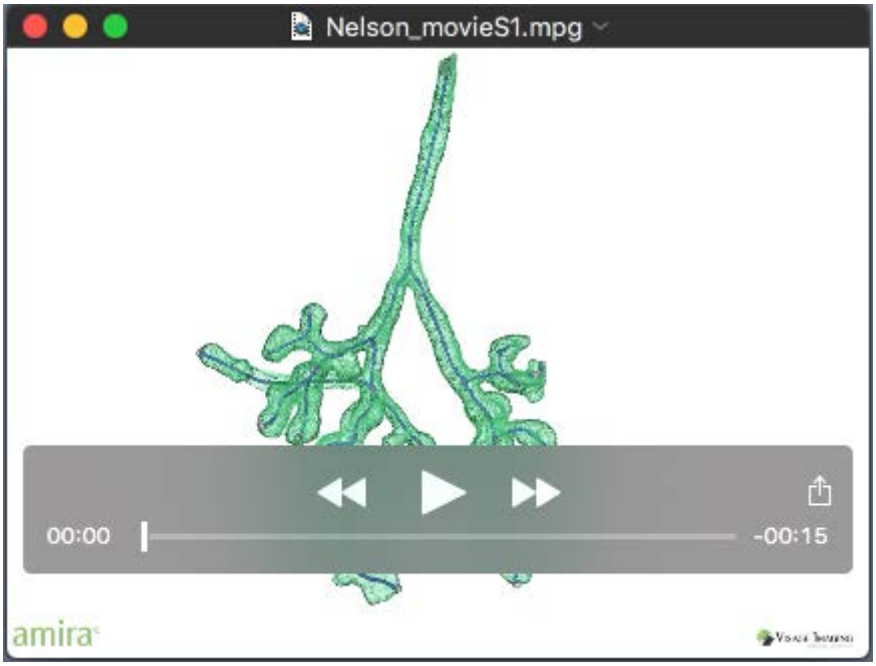

Supplemental Movie 1. Example 3D reconstruction of confocal image stacks using Amira software for lung explant presented in Figure 1E. Epithelium is shown in green; skeletonization of major branches is indicated by a blue line for clarity.

Development • Supplementary information

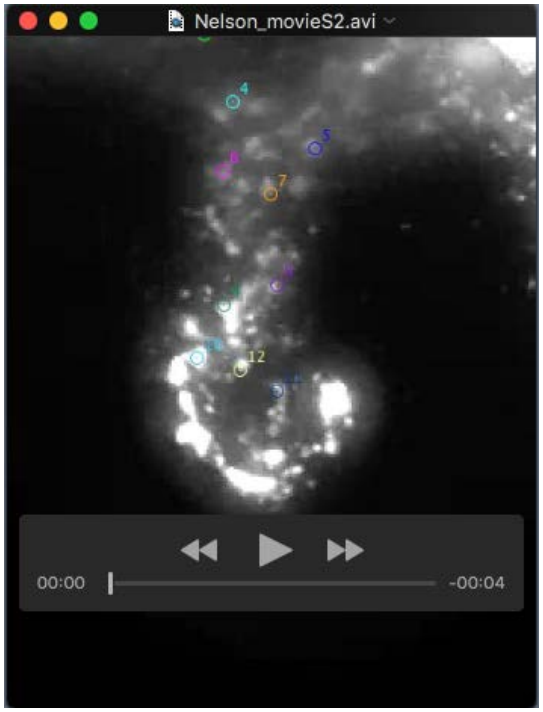

Supplemental Movie 2. Timelapse movie of the flow of fluorescent tracer particles within the lumen of the airways, as shown in Figure 3F.

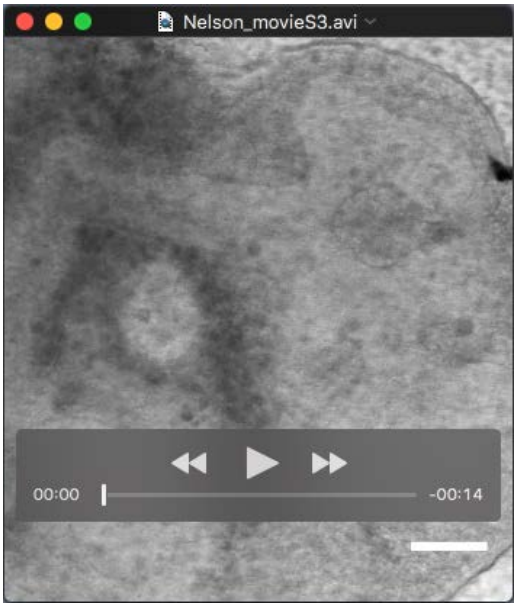

Supplemental Movie 3. Treatment with nifedipine blocks airway smooth muscle contraction.

Development • Supplementary information

Supplemental Figures

Supplemental Figure 1

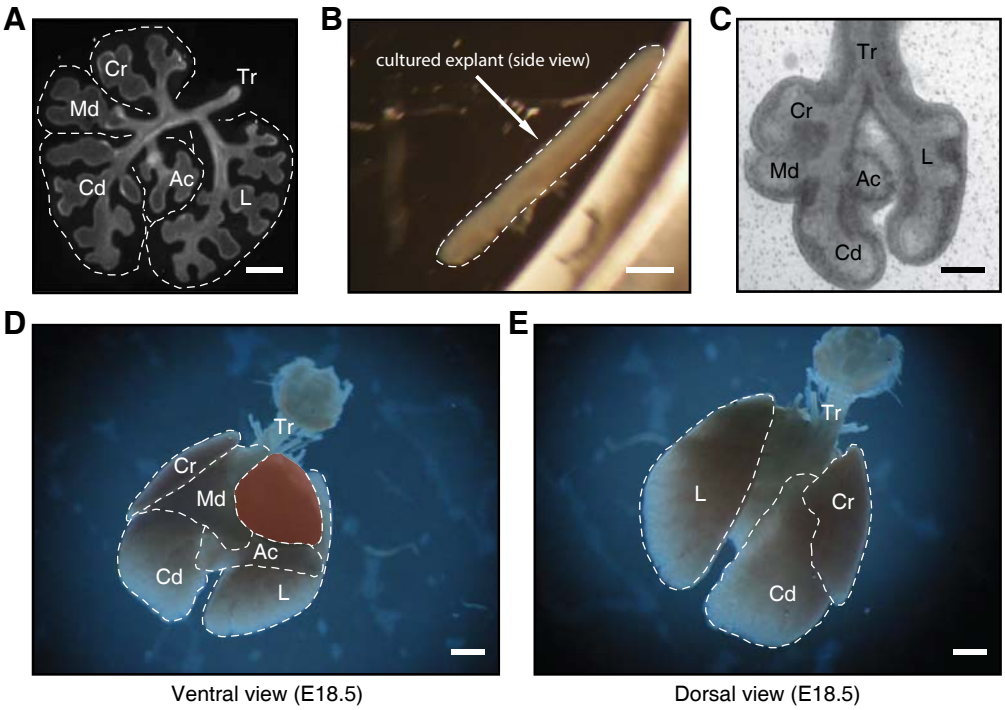

Supplemental Figure 1: (A) E-cadherin staining of airways from an explant cultured for 48 hours on a floating porous membrane. (B) Side profile view of a fixed lung explant cultured on a floating porous membrane, demonstrating that the organ grows and develops into a planar structure. Lobes of the murine lung labeled for explants at (C) early stages of development (~*E*12.5) and (D, E) late gestation (*E*18.5). Tr, trachea; L, left lobe; Cr, cranial lobe; Md, middle lobe; Cd, caudal lobe; Ac, accessory lobe; dotted lines in panels A, D, and E outline the boundaries of the lobes. Scale bars: 200 μm in A, B, and C; 500 μm in D and E.

Development • Supplementary information

Supplemental Figure 2

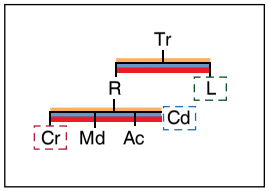

ΔP = 20 Pa, ΔP = 100 Pa, ΔP = 200 Pa, *in vivo*

Cr See Figure 2C

terminal branches per lobe

lobe \ ΔP	20 Pa	100 Pa	200 Pa
Cr	6	12	16
Cd	6	13	24
L	5	10	15

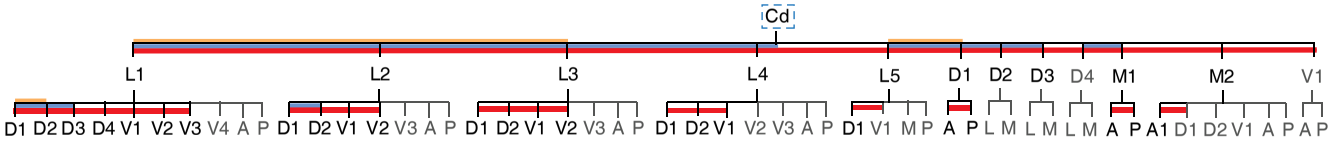

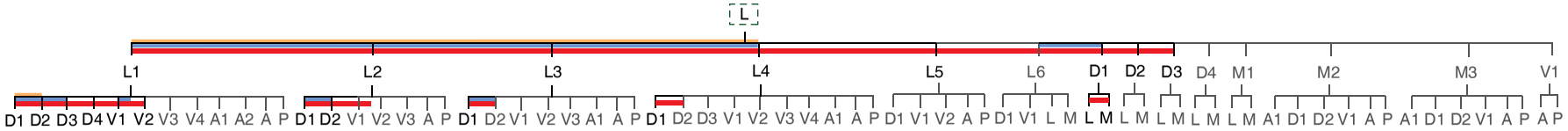

Supplemental Figure 2: Lineage diagrams for explants cultured unde ΔP of 20 Pa (orange), 100 Pa (blue), and 200 Pa (black) compared to late gestation explants *in vivo* (gray). Table shows number of branches per lobe for explants held under each ΔP.

Development • Supplementary information

Supplemental Figure 3

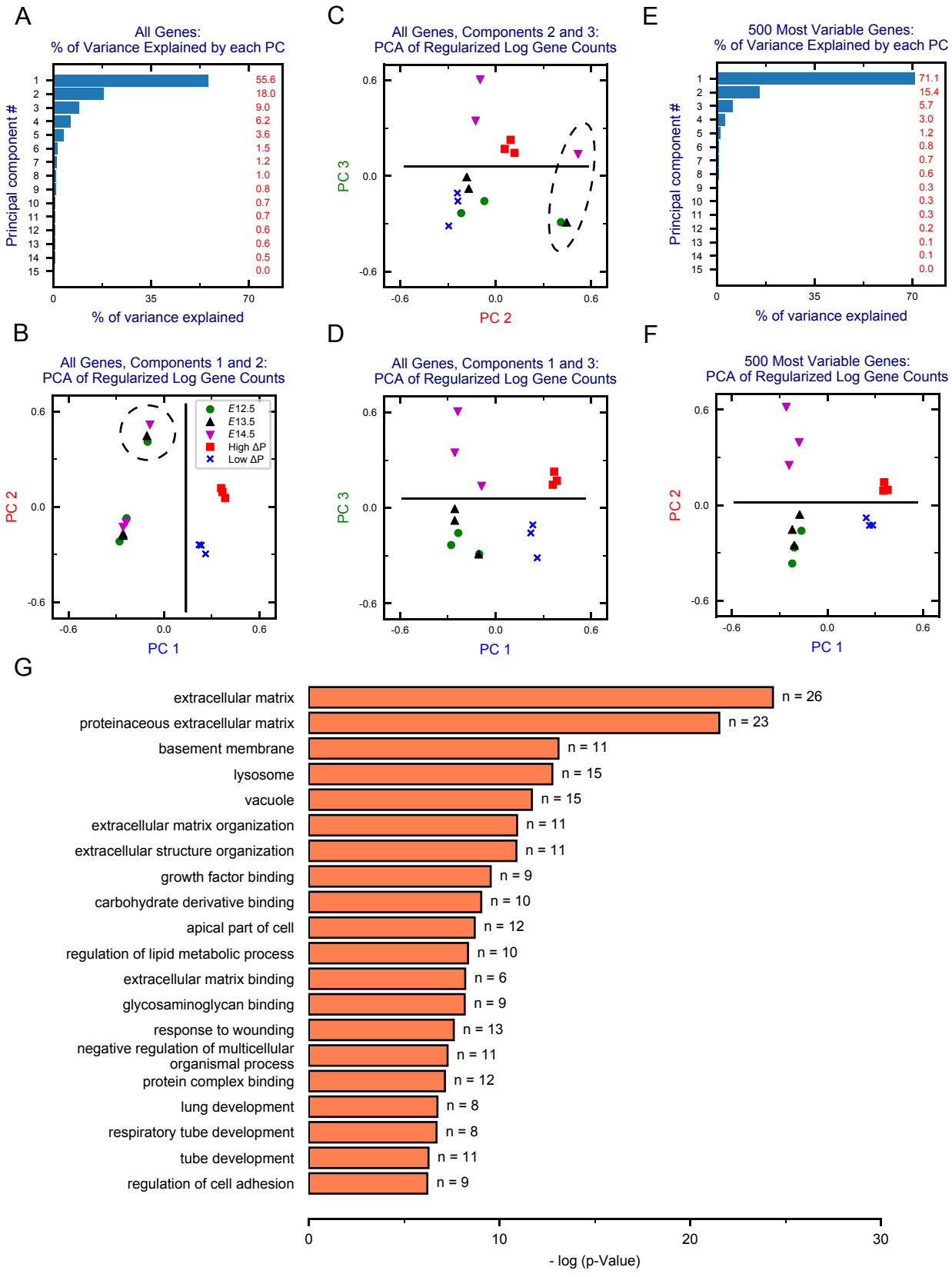

Development • Supplementary information

Supplemental Figure 3: (A-D) Principal component analysis on all genes from three biological replicates of each condition. (A) The percent of variance explained by each of the 15 principal components. (B) First and second principal components of each sample. The vertical line illustrates the separation along principal component 1 between lungs *in utero* and those cultured in microfluidic chest cavities. The dashed circle marks a batch effect in the second principal component for three samples that were sequenced at a different time than the others. (C) Second and third principal components of each sample. The horizontal line illustrates how *E*14.5 and high ΔP lungs separate from *E*12.5, *E*13.5, and low ΔP lungs along the third principal component. The dashed oval is the same as the circle in (B). (E-F) PCA analysis on the 500 genes with the highest variance across each condition. (E) The percent of variance explained by each principal component. (F) The first two principal components. The horizontal line illustrates how *E*14.5 and high ΔP lungs separate from *E*12.5, *E*13.5, and low ΔP lungs along the second principal component. (G) Top 20 gene ontology groups enriched among genes significantly increased in lungs both at *E*14.5 (vs *E*12.5) and under high (vs low) ΔP. n = number of genes from each group in this overlap (out of 216 total).

Development • Supplementary information

Supplemental Figure 4

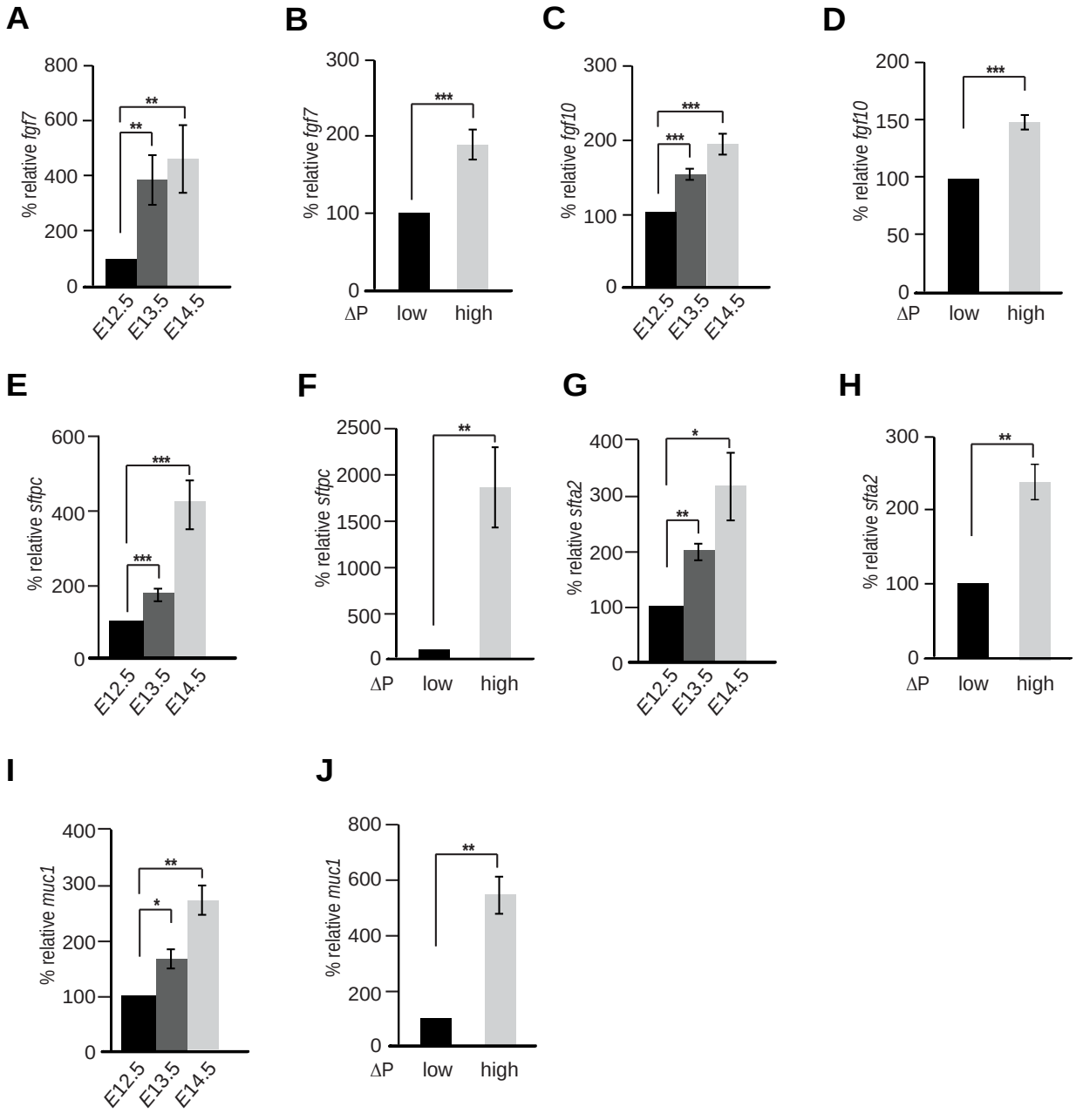

Supplemental Figure 4: High transmural pressure induces expression of genes that drive airway morphogenesis and maturation. Relative transcript levels of (A, B) *fgf7*, (C, D) *fgf10*, (E, F) *sftpc*, (G, H) *sfta2*, and (I, J) *muc1* for lungs isolated at *E*12.5, *E*13.5, and *E*14.5 or held under low or high ΔP. Error bars represent s.e.m. for experiments conducted in triplicate. (*) P<0.05; (**) P<0.01; (***) P<0.001.

Development • Supplementary information

Supplemental Figure 5

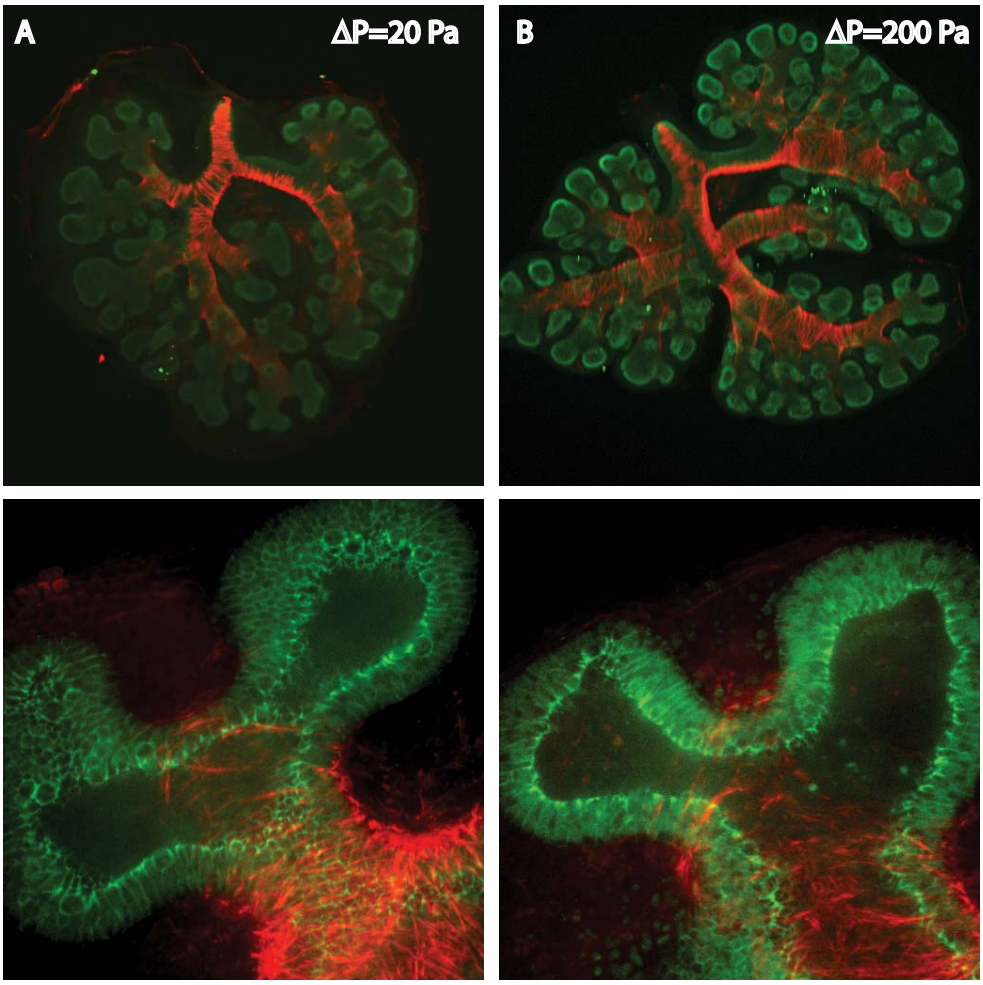

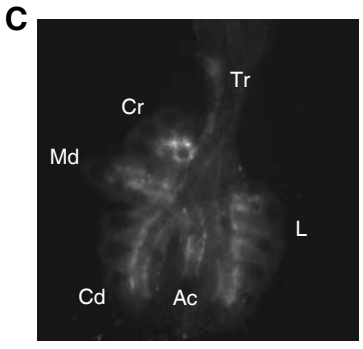

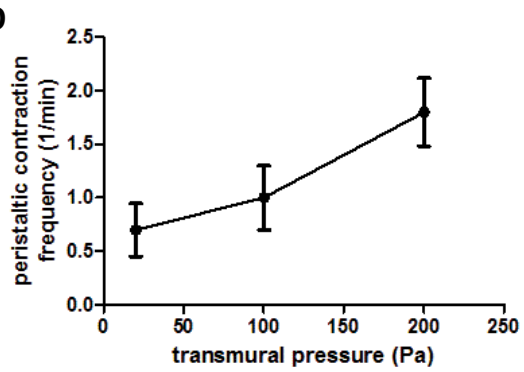

Development • Supplementary information

Supplemental Figure 5: Transmural pressure enhances smooth muscle development. (A, B) Immunofluorescence staining of E-cadherin (green) and αSMA (red) in explants cultured under ΔP of 20 or 200 Pa. (C) Image of an explanted lung from αSMA-RFP transgenic mouse embryo. This fluorescence signal delineates the developing airway smooth muscle at the outer boundaries of the airways and enables the observation of airway contractions. (D) Peristaltic contraction frequency of the proximal airways as a function of transmural pressure.

Development • Supplementary information

Supplemental Figure 6

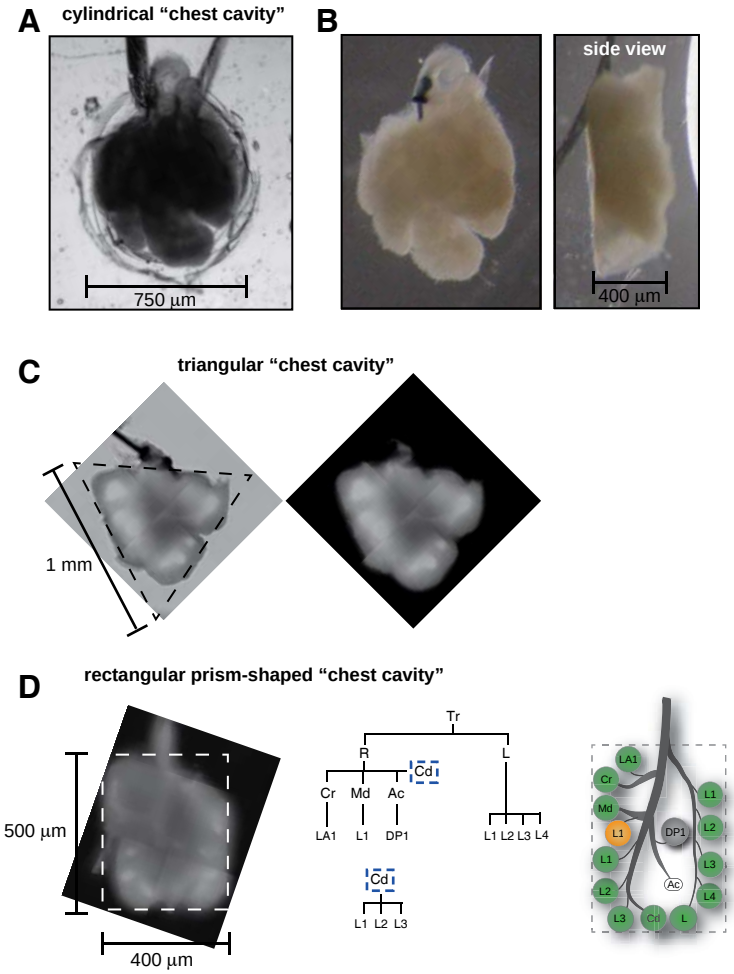

Supplemental Figure 6: The shape of the chest cavity determines the gross morphology of the lung. (A) Lung explant cultured for 48 hours within a cylindrical chest cavity and (B) brightfield images of front and side view of a representative explant. (C) Brightfield image and fluorescent image (E-cadherin) of a lung explant cultured within an equilateral triangle-shaped chest cavity (1-mm per side, 400 µm deep). (D) Fluorescent image of a lung explant cultured within a rectangular prism-shaped chest cavity (500 µm x 400 µm x 400 µm deep) and the corresponding lineage diagram and schematic showing the final location of the branches within the cavity.

Development • Supplementary information